IOPscience iopscience.iop.org

Home Search Collections Journals About Contact us My IOPscience

Integration of nano-scale components and supports in micromachined 3D silicon structures

This content has been downloaded from IOPscience. Please scroll down to see the full text.

2014 J. Micromech. Microeng. 24 045008

(http://iopscience.iop.org/0960-1317/24/4/045008)

View the table of contents for this issue, or go to the journal homepage for more

Download details:

IP Address: 137.132.123.69
This content was downloaded on 05/08/2014 at 04:29

Please note that terms and conditions apply.

IOP Publishing

Journal of Micromechanics and Microengineering

J. Micromech. Microeng. **24** (2014) 045008 (9pp)

doi:10.1088/0960-1317/24/4/045008

Integration of nano-scale components and supports in micromachined 3D silicon structures

J Song[1], S Azimi[1], Z Y Dang[1] and M B H Breese[1,2]

[1] Department of Physics, Centre for Ion Beam Applications (CIBA), National University of Singapore, Singapore 1175422

[2] Singapore Synchrotron Light Source (SSLS), National University of Singapore, 5 Research Link, Singapore 117603

E-mail: phymbhb@nus.edu.sg

Received 18 November 2013, revised 27 January 2014
Accepted for publication 28 January 2014
Published 10 March 2014

Abstract

We have developed a process for the three-dimensional (3D) machining of p-type silicon on a micro- and nano-scale using high-energy ion beam irradiation with one or more energies and fluences, followed by electrochemical anodization in hydrofluoric acid. We present a study of the dependence of our fabricated structures on irradiating ion energies, fluences, geometries and wafer resistivity. All these factors determine whether the micro- and nano-scale features are properly connected to the supports in the 3D silicon structures. If wrongly chosen, any of these factors may cause a breakage at the connection through localized over-etching. Under optimum irradiation and anodization conditions, free-standing patterned membranes can be fabricated with feature dimensions of 100 nm over areas of many square millimeters. This investigation is based on silicon structures but is relevant to any electro-assisted etching process for 3D fabrication, paving the way for achieving free-standing silicon photonics, mechanical resonators and micro-/nano-electromechanical systems.

Keywords: 3D nano-scale silicon machining, electrochemical anodization, ion irradiation, silicon nanostencils, free-standing membranes

(Some figures may appear in colour only in the online journal)

1. Introduction

We have developed a process involving ion beam irradiation followed by electrochemical anodization for machining p-type silicon on a micro- and nano-scale [1–4]. These three-dimensional (3D) structures can be used in a range of research and technological areas, such as silicon photonics [2–5], thermal or defect property studies [6] or nano-electromechanical systems [7, 8]. While there are many other silicon machining processes available, ours is unique in being able to directly machine silicon in three dimensions, leaving the surface layers intact while creating one or more patterned levels beneath the surface [1, 4]. Other processes require many repeated steps to build up such 3D geometries [9–11].

To create such 3D structures, low fluence ion irradiation (typically 10^{14} to 10^{15} ions cm^{-2}) with proton energies of 50 to 500 keV is used to create sub-surface regions of damage, which form the micro- and nano-scale components. These ions come to rest at their end-of-range depth (0.6 to 6 μm) beneath the wafer surface, figure 1. The ion irradiation of a crystalline material results in displacement damage owing to the nuclear stopping component of the energy loss [12, 13], in which lattice atoms are displaced away from their initial locations. In p-type silicon, some of these defects act as hole traps [14–18], reducing the free carrier density and inducing a positive repulsive potential at the irradiated region which alters the subsequent flow of current through it [19]. Above a certain fluence the free carrier density is reduced to zero. At this point the irradiated material does not undergo electrochemical

 © 2014 IOP Publishing Ltd Printed in the UK

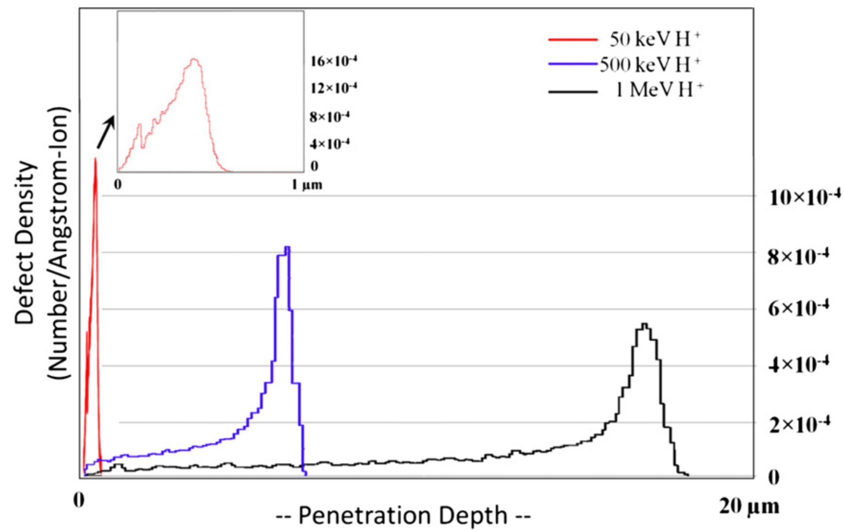

Figure 1. SRIM plots of the defect density versus depth for 50 keV, 500 keV and 1 MeV protons.

anodization [20, 21], with the local anodization current being partially or completely deflected around irradiated regions [18, 19]. At high fluences, the full ion trajectory is depleted and the thickness of the remaining crystalline silicon is similar to the ion range. Since the rate of nuclear energy loss increases as the ions lose energy, more defects (typically an order of magnitude more) are created close to the end-of-range depth, figure 1, so at low fluences only this region remains unanodized, while those regions closer to the surface form porous silicon during anodization. Anodization past the end-of-range of such low-fluence-irradiated regions results in crystalline silicon regions which are completely surrounded by porous silicon. This process has been used to make a variety of 3D structures which remain embedded in porous silicon, or if the porous silicon is removed by immersion in KOH the 3D structure is revealed. A similar ion irradiation may also be applied to other compound semiconductors such as GaAs and InP [22, 23].

Fabrication of 3D structures using this process usually requires a combination of patterning of micro- and nano-scale features and larger support bars to hold them in place after the surrounding porous silicon has been removed. It was noted early during the development of this process that the supported features tended to fracture at the connecting point with the larger, more robust support bars. The motivation of this work is to consider how best to integrate such fine-scale features produced by low fluences of low energy ions, with larger, coarser-scale support bars made from high fluences of higher energy ions. We study the conditions under which the connecting point between fine- and coarse-scale patterns are best made, and explain the observed behavior in terms of the current flow during anodization.

2. Experiment

There are three basic geometries of 3D structures which can be made using this process. First, a fine-scale pattern is created by low fluence irradiation with, e.g. 50 keV protons through a 1 μm thick polymer surface mask, such as PMMA (polymethyl methacrylate) which is patterned using electron beam lithography [24]. The same polymer resist can also be patterned using the same e-beam process to incorporate support bars, typically 1 to 5 μm in width, which are used to hold the nano-scale features in place over small distances. In this case the fine-scale features and support bars are created by the same areal fluence of irradiation, figure 2(*a*), since they are exposed to the same ion flux for the same period. After anodization beyond the ion end-of-range the fine-scale features are completely undercut but remain attached to the substrate by the support bars which are not undercut because they are wider. Since the final structure remains attached to the substrate, it is not subjected to external handling.

In the second 3D geometry a fine-scale pattern is created using low-fluence proton irradiation through an e-beam-defined surface mask, in the same manner as above, or using direct-write-focused beam irradiation for higher ion energies. The structure created by this pattern is held in place by a coarse network of robust support bars of a few microns in width. These are created by a high fluence of MeV protons with a range of 3 to 50 μm. During deeper anodization, all the fine-scale lines and support features which are irradiated by low energy ions are completely undercut. Anodization is stopped before the high-energy support structure is undercut in order to leave the fine-scale features attached to the substrate (figure 2(*b*)). From figure 1 the defect density created close to the surface is considerably reduced at higher ion energies, so deep supports must be irradiated with a higher proton fluence in order to introduce a sufficiently high defect density to ensure that they are not significantly etched.

If anodization is further continued then one may completely undercut the support structure, allowing the 3D membrane to be completely separated from the substrate after immersion in KOH to remove all porous silicon, figure 2(*c*). The coarse mesh provides a rigid support to a free-standing membrane, allowing it to be manipulated and mounted as appropriate and used as a stencil for lithography [25–28] or a free-standing photonic lattice, or a variety of other

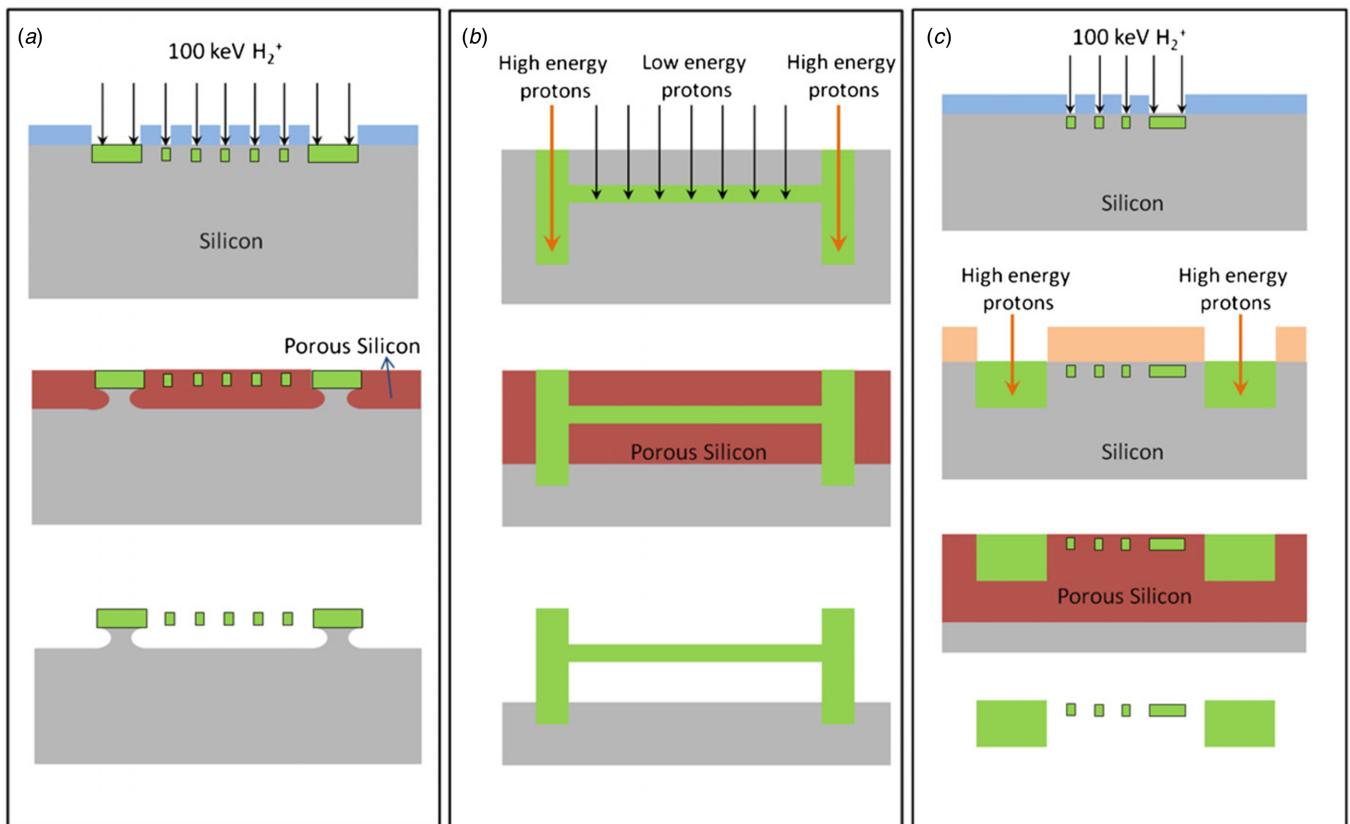

Figure 2. Schematic of the experimental steps for fabricating free-standing silicon nanostructures and support structures with (*a*) single energy (*b*) different ion beam energies and (*c*) both processes for free-standing patterned membranes. The final 3D structure is shown in green, porous silicon is red and the e-beam defined photoresist in light blue.

applications. One significant difference with this type of structure compared to that in figure 2(*b*) is that the coarse supports tend to be wider, typically 10 μm, and shallower, typically 3 μm. The shallower depth is because they are normally irradiated with helium ions to take advantage of their greater defect production rate, and their greater width is to impart additional rigidity to the free-standing membrane.

3. Results and discussion

Figure 3 shows arrays of nano-scale lines and fine-scale support bars which were fabricated according to figure 2(*a*), in 0.4 Ω cm (i.e. 'high' resistivity) and 0.02 Ω cm silicon (i.e. 'low' resistivity) p-type wafers. For ease of studying the different effects which are produced by ion irradiation it is convenient to consider different regimes of resistivity, i.e. high or low, in order to assess what problems occur in each and what different attributes they have, but in practice there is no rigid distinction between the effects that are observed. In particular, for high-fluence irradiation of low resistivity wafers, the observed behavior during anodization is similar to that of high resistivity wafers, as discussed below.

Figures 3(*a*), (*b*) show plane views of the patterned structures which were defined using an e-beam patterned PMMA polymer resist, which was thick enough to stop the subsequent 50 keV proton irradiation (range in PMMA 0.8 μm, range in silicon 0.6 μm). Irradiation of the exposed wafer surfaces results in both nano-scale features and support bars with the same areal fluence. An anodization depth of 2 μm is enough to fully undercut the nano-scale features, while leaving the 2 μm wide support bars (vertically-running in figure 3(*a*)) attached to the substrate. There are still wider supports, to which the 2 μm wide support bars are connected (horizontally-running in figure 3(*a*)), but these are not discussed here.

Figure 3(*c*) shows a cross-section of the 2 μm wide support bars. In the unirradiated 0.4 Ω cm wafer the hole density is low, so a low fluence ion irradiation is sufficient to induce enough hole traps to significantly reduce the hole density close to zero, resulting in a large, built-in positive potential along the full ion trajectory [19]. This strongly deflects all electrochemical drift current around it during subsequent anodization, leaving the full volume of the irradiated support as unetched, remaining as crystalline silicon. In comparison, the nano-scale lines have a smaller height, approximately equal to the depth distribution of the end-of-range defect peak (figure 3(*e*)). The difference is due firstly because anodization current can flow around a narrow end-of-range widths of a few hundred nanometers, whereas it cannot do so for wider end-of-range features. The greater thickness of the support bars makes them rigid enough to fully support the thinner, nano-scale bars.

The second important difference lies in considering that the same areal fluence irradiating nanoscale patterned widths of about 100 nm and support widths of 2 μm results in

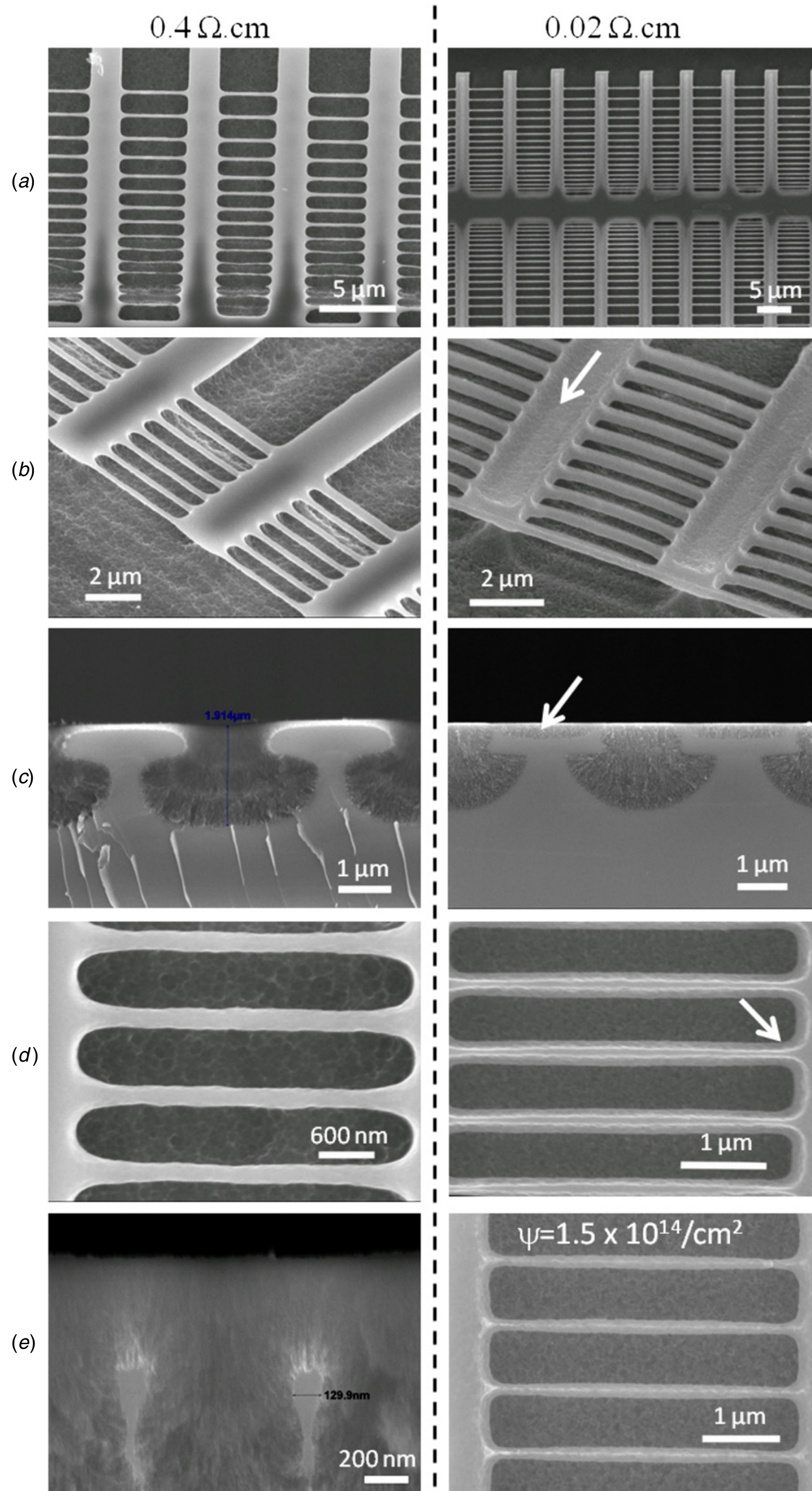

Figure 3. SEM images for 50 keV proton irradiated silicon in (left) 0.4 Ω cm wafer and (right) 0.02 Ω cm wafer. $\psi_a = 2.5 \times 10^{14}$ cm^{-2} except in (*e*) where it is 1.5×10^{14} cm^{-2} for the 0.02 Ω cm wafer. Plan view of nanolines with (*a*) varying period and (*b*) fixed period of 800 nm, held in place by 2 μm-wide supports. Anodization depth of 1 μm. (*c*) Cross-section SEMs of structures comprising similarly irradiated supports of width 1 μm with a separation of 2 μm. (*d*) Higher magnification plan-view image. (*e*) Cross-section of small core size in 0.4 Ω cm wafer, and plan view of 0.02 Ω cm wafer at a lower fluence, where the narrowing of the lines at the connecting points is more obvious.

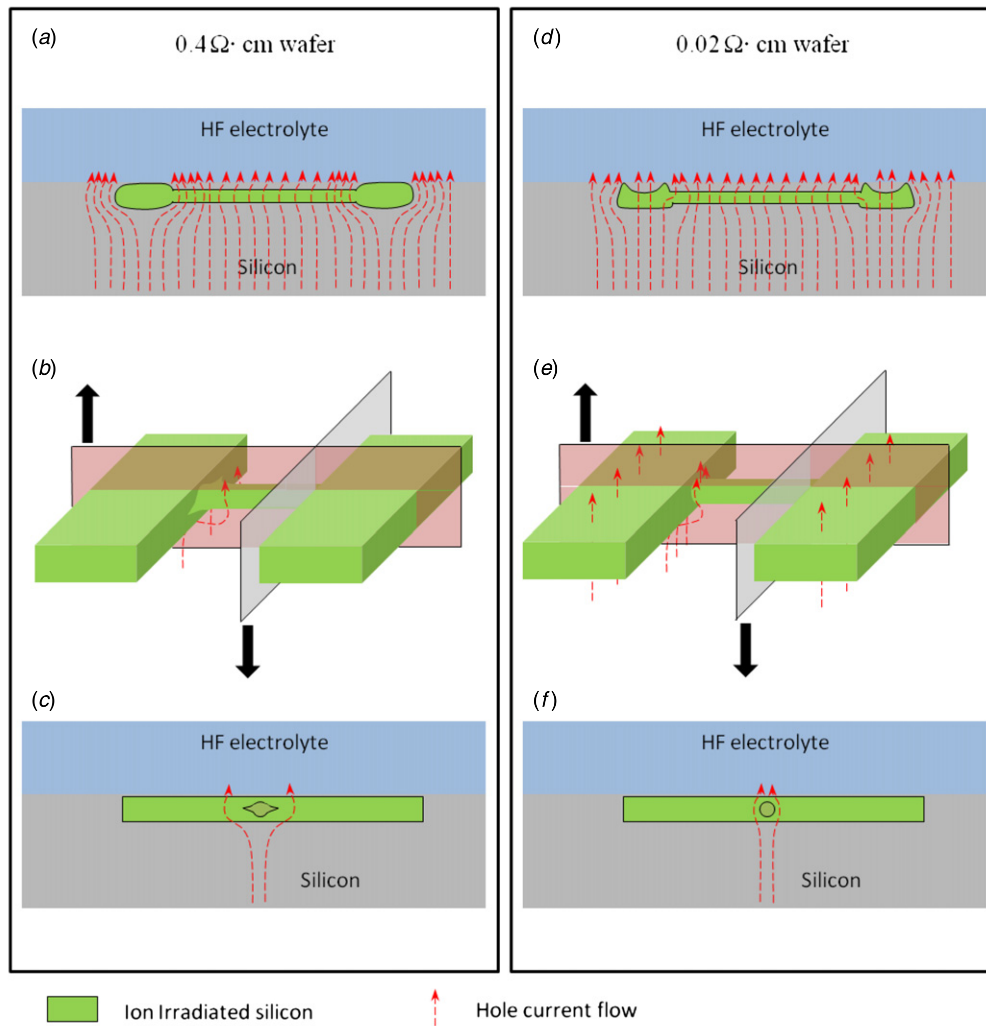

Figure 4. Schematic of current flow during anodization around nano-scale bars and supports in 0.4 Ω cm wafer and 0.02 Ω cm wafer, showing the anodization current flow through and around support bars and the nanobar connecting point. The upper and lower rows show two different cross-sectional views of current flow around the geometry shown in middle row, which indicates the two grey planes at which the cross-sections are shown from this geometry.

different defect densities within the end-of-range region. A narrow irradiated surface area of 100 nm is less than the width of the end-of-range distribution of the defects, so the defect density is less than at wider regions where the areal fluence, ψ_a, irradiating the surface is the same. This point was considered in more detail in [24, 29], and the concept of line fluence, ψ_l, was defined as the number of ions used for irradiating a line of zero width per centimeter of line length. We use the unit of line fluence for irradiating narrow surface widths used for fabricating the nano-scale features and areal fluence for the supports.

Ideally there is no influence of the fine-scale or coarse-scale support bars on the nano-scale features, but in practice there are significant effects which differ in the two wafer resistivities. In the 0.4 Ω cm wafer the fine-scale lines also have a strong repulsive potential, which limits the minimum line spacing in this resistivity to about 700 nm for the anodization current density used [24]. For smaller line spacings the strong repulsive potentials at adjacent bars prevent any current flow so the whole region is unetched. A further consequence is that where the nano-scale bars join the supports, the superposition of the two potentials results in large deflection of the anodization current away from both features, resulting in a large radius of curvature at the connecting point, see figure 3(*d*), where their diameter increases significantly toward the support bar. This effect is shown schematically in figure 4(*c*) by a cross-sectional view of the nano-scale bars at the connection point.

In comparison, in the 0.02 Ω cm wafer, owing to the larger carrier density, a weaker potential is induced by the same ion irradiation as in 0.4 Ω cm wafer. Where the nano-scale bar joins the support bar, the superposition of a second, weak potential results in only a small additional deflection of the current away from the connecting point, see figure 4(*f*). Hence the radius of curvature of the connection of the nano-scale bar to the support is small, figure 3(*d*). The weaker ion irradiation induced potential also makes it difficult to completely stop current flow through the irradiated region, seen in figure 3(*c*). A portion of the anodization current is deflected around the irradiated region whereas some still passes through, with a well-defined reduction of etch rate versus increasing fluence of large areas [30]. The etching of the support bars for the

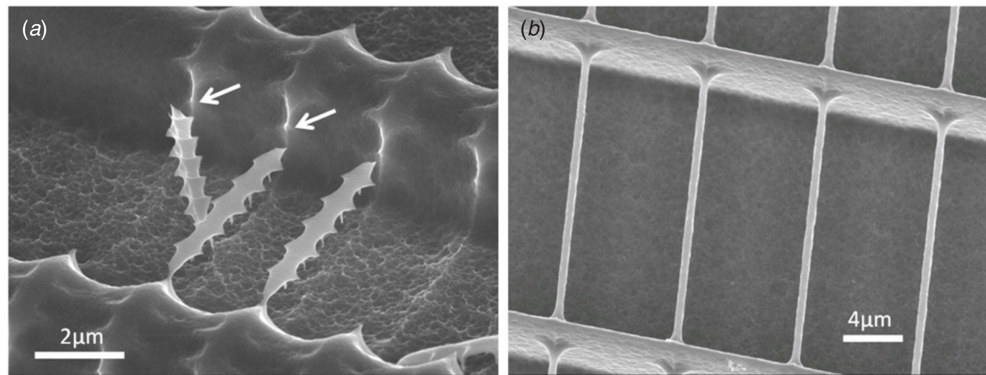

Figure 5. SEM images of examples where different proton beam energies were used to create nanobars in a 0.4 Ω cm wafer which are held in place by high-energy supports (see figure 2(*b*)). (a) Nanobars: 50 keV, $\psi_l = 6 \times 10^9$ cm^{-1}, supports: 500 keV, $\psi_a = 2.5 \times 10^{15}$ cm^{-2}, etch depth of 2 μm. (b) Bars: 500 keV protons, $\psi_l = 1.8 \times 10^9$ cm^{-1}. Supports: 1 MeV, $\psi_a = 1.5 \times 10^{16}$ cm^{-2}. Etch depth of 12 μm.

0.02 Ω cm wafer is shown by arrows in figures 3(*b*), (*c*). This effect varies across the width of an irradiated area, figure 4(*d*), a larger fraction of the hole current which flows toward the center of the irradiated area passes through it compared to current flowing closer to the edges where it is easier for current to be deflected around the outer edge, leaving the edge region less deeply anodized than the center. This same effect was observed for parallel rows of closely spaced nano-scale bars [22].

However, the component of the hole current that flows through the support bars in the 0.02 Ω cm wafer may reach the surface close to, or even within, the connecting point with the nanobar, or even along it. This results in localized etching of the nanobar close to the support, see the arrowed location in figure 3(*e*) where the bar width at this location is smaller than toward the center. This effect is consistently observed in the low resistivity wafer, and is shown schematically in figure 4(*d*).

In figure 3(*e*) for the 0.02 Ω cm wafer the fabrication process is the same as above but a lower fluence of 1.5×10^{14} cm^{-2} was used. The thinning at the connection point is more pronounced. From this, one can conclude that narrow diameter, free-standing bars can be fabricated in the 0.4 Ω cm wafer, down to 50 nm [24], since there is no limitation caused by anodization current flowing into them through the supports. In comparison, for the 0.02 Ω cm wafer, reducing the fluence results in a high likelihood of the connection failing due to current flowing through the support bar, so one cannot make such small diameter, free-standing wires.

Therefore the shape of the nanobars close to where it joins a support depends on two effects, namely 'inside current flow' due to the component of the hole current which flows through the support, into the connection part; 'outside current flow' owing to deflection of the current around the support. Inside current flow narrows the connecting point, which works from the initial anodization till the end, inducing worse results with longer etching time. In figure 3, none of the nano-scale bars have broken, but if anodization proceeds to a greater depth then the connecting points can become too thin to support the nano-scale bar, causing their breakage as discussed further below. In comparison, outside current flow plays a part only when the etching front evolves through the nano-scale bar depth. Once the nanobars are undercut, the deflection current flows directly into the electrolyte instead of influencing the shape of the nanobars. On one hand, as discussed in figure 3, the deflected current by the support and nanobars broadens the connection part. On the other hand, it can induce an opposite effect, namely narrowing the connection part, if the built-in potential of the nanobars is not large enough to deflect this current away again, which will be discussed below.

Now consider the geometry in figure 2(*b*), where low fluence irradiated nano-scale features are held in place by high-energy, high-fluence supports which are intended to provide a robust frame to hold the nano-scale features in place over large patterned areas. The wafer may be deeply anodized, up to 20 μm, depending on the ion type, energy and geometry of the supporting structure. There are two important considerations as to why a much higher ion fluence is required to fabricate the robust supports. First, because higher energy ions are used, the defect density close to the surface, where etching is most likely to occur, is lower than for the same fluence of low energy ions, figure 1, requiring a higher fluence to achieve a similar defect density. Second, because of the greater etch depth, the inside current flow effect is more obvious, the defect density needs to be higher, hence the fluence used for the coarse support bars needs to be higher than that used for the fine-scale supports in figure 2(*a*), in order to adequately prevent the flow of current from entering the support and exiting at the nanobar connection.

An example of this effect is show in figure 5(*a*) where the fluence used to fabricate the supports is an order of magnitude greater than that used in figure 3. However, even though the etch depth is only 2 μm the top surface has undergone significant etching as the defect density is not high enough to prevent current flowing into them and breaking all the nanobars. Note the periodic etching along the support, where the additional fluence due to the irradiation to define the nanobars locally reduces the etch rate, a clear indication that the fluence used to irradiate the support is too low. Figure 5(*b*) provides an example where a fluence of two orders of magnitude greater than in figure 3 was used to irradiate the supports. This now results in uniform diameter nanowires produced over ten micrometer lengths though with the characteristic broadening at the connecting point with the support.

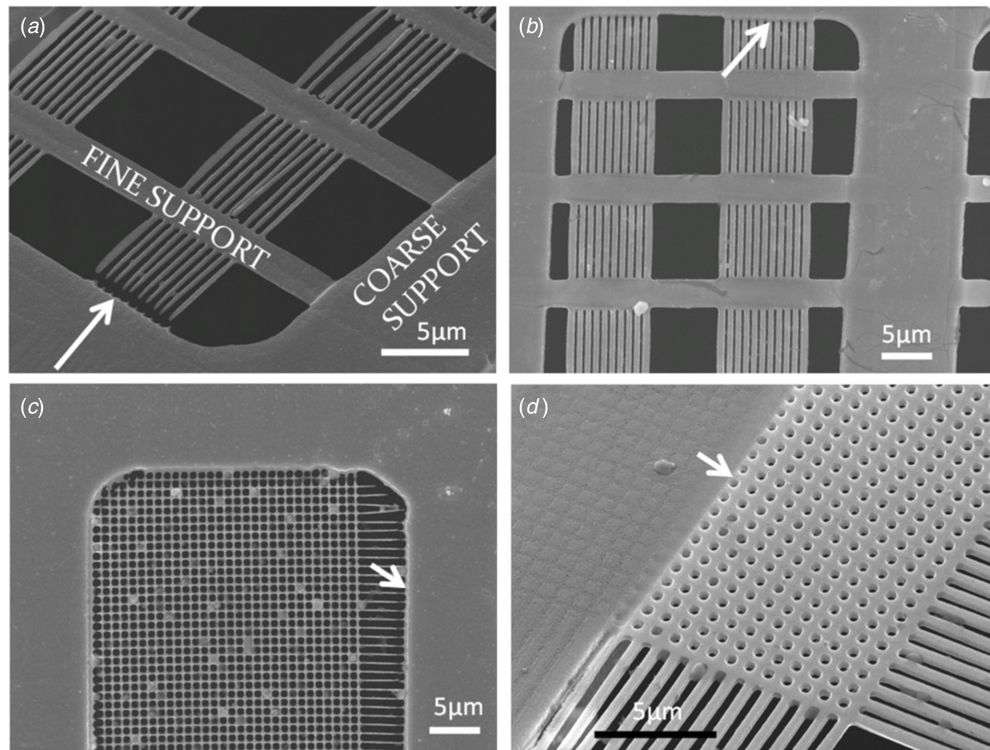

Figure 6. SEM images of free-standing patterns of silicon structures in 0.02 Ω cm wafer where the coarse period helium supports are all written with $\psi_a = 2 \times 10^{15}$ cm^{-2}. (*a*), (*b*) Nano-scale patterns irradiated with $\psi_a = 1 \times 10^{15}$ cm^{-2}. (*a*) 650 nm line period, $\psi_l = 9 \times 10^9$ cm^{-1}, etched at 100 mA cm$^{-2,}$ (*b*) 850 nm line period, $\psi_l = 2 \times 10^{10}$ cm^{-1}, etched at 60 mA cm^{-2}. (*c*), (*d*) Both with 850 nm line period, etched at 60 mA cm^{-2}. (*c*) $\psi_a = 4.5 \times 10^{14}$ cm^{-2}, $\psi_l = 4 \times 10^9$ cm^{-1}, (*d*) $\psi_a = 8 \times 10^{14}$ cm^{-2}, $\psi_l = 7.2 \times 10^9$ cm^{-1}.

The third type of 3D structure considered here is a further development of that described above, as shown in figure 2(*c*). Again a patterned array of nano-scale bars and supports is supported by a coarser mesh of supports produced by higher energies. Now the full structure is separated from the substrate by immersion in KOH, forming a patterned membrane, comprising nano-scale bars and fine-scale supports which are, in turn, connected to a coarse supporting structure. These separated membrane structures were fabricated in the lower resistivity wafer, as this has proven more useful for nano-scale patterning, suffering less problems with less cracking of the porous silicon, a small radius of curvature of connecting joins, smoother surfaces and smaller gaps of only 100 nm between adjacent features, compared to 700 nm in the higher wafer resistivity. However, a drawback of this wafer resistivity is its greater tendency to suffer from problems related to anodization current flow through the irradiated structure, as described above. Successful fabrication of this type of 3D structure simply depends on understanding the effect of the various fluences and pattern geometries on the anodized structure.

In figure 6, the coarse period helium supports are all written with an areal fluence of 2×10^{15} cm^{-2} 1 MeV helium ions, which are used as a high defect density is required to prevent any etching in the low resistivity material. While this could be achieved with protons, as for the structures in figure 5 for the higher resistivity material, above a certain fluence it becomes easier to use helium ions owing to their greater rate of defect production. 1 MeV helium ions have a similar range ($\sim$3 μm) and defect depth distribution as 250 keV protons, but produce about 20 times more defects owing to the higher ion mass. Under the effect of such a high helium ion fluence, the hole density within the low resistivity material is very low and the irradiated regions now effectively act the same as those in 0.4 Ω cm material where anodization current is deflected around the irradiated areas. Since the coarse supports are wide ($\sim$10 μm) then a large current is deflected around them and flows to the surface close to the side walls; this large deflected current now causes another type of problem at the connecting points as the nanolines do not contain a large built-in potential which is able to deflect this current away, as occurs for the 0.4 Ω cm material, so are prone to be dissolved away more easily. Thus, although a support which is irradiated with high fluence has the advantage of preventing the flow of current entering the support, it deflects larger current around at the same time. In the case that the outside current flow effect is enhanced, the ratio between the nanolines and support needs to be considered, in order to ensure that the nanolines have the comparable ability to deflect the current away instead of being dissolved.

An example of where this type of 3D nanostructure has failed for this reason is shown in figure 6(*a*), where an array of nano-scale bars is successfully supported by fine-scale supports, see the upper arrow, but where it joins the coarse support it fails, shown by the lower arrow. The nano-scale bars are fully anodized slightly away from the support wall by the large current which is deflected around the coarse support, whereas the wider nano-scale supports are left successfully

attached to the coarse support. This problem can be avoided by using a higher fluence to irradiate the fine-scale features and also a slightly larger line period [24], both of these factors resulting in the nanobars having a larger diameter and so are able to withstand anodization without being dissolved away, figure 6(*b*). Similarly, figures 6(*c*), (*d*) shows another example where lines or a grid are etched away close to the support (c). In figure 6(*d*) this problem was solved by using a higher fluence, with the lines remaining attached to the support.

4. Conclusion

In conclusion, we have shown that there are different considerations in designing each level within a multilevel structure, and in particular for free-standing membranes care must be taken to design the structure, based on an understanding of how each level is influenced by others. Achieving a successful 3D structure necessitates several factors to be considered: an interior current flow induces a localized over-etching at the connection between nanobars and support structures. It flows from the start of anodization till the end, inducing worse performance with longer etching time. It can be mitigated by increasing the fluence used for the supports or shortening the etching time. An outer current flow is present due to the deflection of the hole current around the support. It may broaden or narrow the connection, depending on the ratio of the fluence used for the nanolines and supports. A proper understanding of these factors is essential to correctly choose the optimum experimental parameters for a given geometry, allowing unique, 3D geometries of nano-scale features to be produced, opening up a variety of new applications in the nanosciences, from stencil lithography to nano-scale photonics and MEMS devices.

Acknowledgments

We wish to thank the International Atomic Energy Agency for partial support under the CRP project no. F11016. This work was partly performed at SSLS under NUS Core Support C-380-003-003-001, and National Research Foundation project NRF-CRP8-2011-06.

References

[1] Azimi S, Song J, Dang Z Y, Liang H D and Breese M B H 2012 Three-dimensional silicon micromachining *J. Micromech. Microeng.* **22** 113001

[2] Teo E J, Xiong B Q, Ow Y S, Breese M B H and Bettiol A A 2009 Effects of oxide formation around core circumference of silicon-on-oxidized-porous-silicon strip waveguides *Opt. Lett.* **34** 3142–4

[3] Yang P Y, Mashanovich G Z, Gomez-Morilla I, Headley W R, Reed G T, Teo E J, Blackwood D J, Breese M B H and Bettiol A A 2007 Freestanding waveguides in silicon *Appl. Phys. Lett.* **90** 241109

[4] Liang H D, Kumar V S, Wu J F and Breese M B H 2013 Ion beam irradiation induced fabrication of vertical coupling waveguides *Appl. Phys. Lett.* **102** 131112

[5] Sun P and Reano R M 2010 Low-power optical bistability in a free-standing silicon ring resonator *Opt. Lett.* **35** 1124–6

[6] Potts A, Williams D A, Young R J, Blaikie R J, Mcmahon R A, Hasko D G, Cleaver J R A and Ahmed H 1990 Fabrication of freestanding single-crystal silicon nanostructures for the study of thermal transport and defect scattering in low dimensional systems *Japan. J. Appl. Phys.* **29** 2675–9

[7] Feng X L, He R R, Yang P D and Roukes M L 2007 Very high frequency silicon nanowire electromechanical resonators *Nano Lett.* **7** 1953–9

[8] Belov M, Quitoriano N J, Sharma S, Hiebert W K, Kamins T I and Evoy S 2008 Mechanical resonance of clamped silicon nanowires measured by optical interferometry *J. Appl. Phys.* **103** 074304

[9] Fischer A C, Belova L M, Rikers Y G M, Malm B G, Radamson H H, Kolahdouz M, Gylfason K B, Stemme G and Niklaus F 2012 3D free-form patterning of silicon by ion implantation, silicon deposition, and selective silicon etching *Adv. Funct. Mater.* **22** 4004–8

[10] Jeon J, Floresca H C and Kim M J 2010 Fabrication of complex three-dimensional nanostructures using focused ion beam and nanomanipulation *J. Vac. Sci. Technol.* B **28** 549–53

[11] Lin S Y, Fleming J G, Hetherington D L, Smith B K, Biswas R, Ho K M, Sigalas M M, Zubrzycki W, Kurtz S R and Bur J 1998 A three-dimensional photonic crystal operating at infrared wavelengths *Nature* **394** 251–3

[12] Ziegler J F, Ziegler M D and Biersack J P 2010 SRIM—the stopping and range of ions in matter (2010) *Nucl. Instrum. Methods* B **268** 1818–23

[13] Ziegler J P B J. F. and Littmark U 2003 *The Stopping and Range of Ions in Solids* (New York: Pergamon)

[14] Svensson B G, Mohadjeri B, Hallen A, Svensson J H and Corbett J W 1991 Divacancy acceptor levels in ion-irradiated silicon *Phys. Rev.* B **43** 2292–8

[15] Svensson B G, Jagadish C, Hallen A and Lalita J 1995 Point defects in MeV ion-implanted silicon studied by deep level transient spectroscopy *Nucl. Instrum. Methods* B **106** 183–90

[16] Hallen A, Keskitalo N, Masszi F and Nagl V 1996 Lifetime in proton irradiated silicon *J. Appl. Phys.* **79** 3906–14

[17] Breese M B H, Grime G W and Dellith M 1993 The effect of ion-induced damage on IBIC images *Nucl. Instrum. Methods* B **77** 332–8

[18] Imai K 1981 A new dielectric isolation method using porous silicon *Solid State Electron.* **24** 159

[19] Azimi S, Dang Z Y, Song J, Breese M B H, Vittone E and Forneris J 2013 Defect enhanced funneling of diffusion current in silicon *Appl. Phys. Lett.* **102** 042102

[20] Lehmann V 2002 *Electrochemistry of Silicon: Instrumentation, Science, Materials and Applications* (New York: Wiley)

[21] Sailor M J 2011 *Porous Silicon in Practice: Preparation, Characterization and Applications* (Weinheim: Wiley)

[22] Menzel F, Spemann D and Butz T 2011 High-aspect ratio microstructures in p-type GaAs and InP created by proton beam writing *Nucl. Instrum. Methods* B **269** 2457–61

[23] Diering D, Spemann D, Lenzner J, Muller S, Bontgen T and von Wenckstern H 2013 Greyscale proton beam writing in p-type gallium arsenide *Nucl. Instrum. Methods* B **306** 275–80

[24] Song J, Dang Z Y, Azimi S, Breese M B H, Forneris J and Vittone E 2012 On the formation of 50 nm diameter free-standing silicon wires produced by ion irradiation *ECS J. Solid State Sci.* **1** 66–69

[25] Deshmukh M M, Ralph D C, Thomas M and Silcox J 1999 Nanofabrication using a stencil mask *Appl. Phys. Lett.* **75** 1631–3

[26] Yan X M, Contreras A M, Koebel M M, Liddle J A and Somorjai G A 2005 Parallel fabrication of sub-50-nm uniformly sized nanoparticles by deposition through a patterned silicon nitride nanostencil *Nano Lett.* **5** 1129–34

[27] Tun T N, Lwin M H T, Kim H H, Chandrasekhar N and Joachim C 2007 Wetting studies on Au nanowires deposited through nanostencil masks *Nanotechnology* **18** 335301
[28] Vazquez-Mena O, Villanueva G, Savu V, Sidler K, van den Boogaart M A F and Brugger J 2008 Metallic nanowires by full wafer stencil lithography *Nano Lett.* **8** 3675–82
[29] Dang Z Y, Song J, Azimi S, Breese M B H, Forneris J and Vittone E 2013 On the formation of silicon wires produced by high-energy ion irradiation *Nucl. Instrum. Methods* B **296** 32–40
[30] Mangaiyarkarasi D, Sheng O Y, Breese M B H, Fuh V L S and Xioasong E T 2008 Fabrication of large-area patterned porous silicon distributed Bragg reflectors *Opt. Express* **16** 12757–63